ASCE
American Society of Civil Engineers

May 2007
Volume 133, Number 5

ISSN 0733-947X
CODEN: JTPEDI

Journal of Transportation Engineering

T&DI
Transportation and Development Institute and Pipeline Division

Parameter Identification and Analysis of a Slab Track System Using 3D ABAQUS Program

Shao-Tang Yen[1] and Ying-Haur Lee[2]

Abstract: The main objective of this study is to conduct in-depth investigations on the parameter identification and convergence study of slab track analysis. The idealized theoretical solutions are first investigated. Together with the principles of dimensional analysis as well as its similarity to a rigid pavement system, several dominating mechanistic variables are identified and numerically verified. A systematic approach was utilized and implemented in a VISUAL BASIC software package to study the effects of mesh fineness and element selections using the ABAQUS three-dimensional (3D) finite-element model (FEM) program. The convergence characteristics of various 3D shell and 3D solid elements are investigated. Several guidelines in mesh fineness and element selections are recommended. This study strives to bridge the gap between the closed-form solutions and the numerical results obtained from 3D FEM analyses so as to expand its applicability to various practical track conditions more realistically.

DOI: 10.1061/(ASCE)0733-947X(2007)133:5(288)

CE Database subject headings: Slabs; Pavements; Finite element method; Stress; Deflection; Dimensional analysis.

Introduction

Due to the superior structural capacity, stability, safety, as well as economic benefits of slab tracks compared to those of traditional rail-ballast counterparts, slab track systems have become more and more popular in recent railway applications (Bilow and Randich 2000). A conventional railroad track system consists of the rails, rail-pad-fastener systems, ties, ballast, and subgrade, whereas a newly developed track slab system utilizes concrete slab instead of the ties and ballast for stronger structural capacity and less future maintenance needs as shown in Fig. 1(a). The design of slab tracks is similar to that of rigid pavements except that "the loads are applied to the rails connected directly to the concrete slab or through rubber booted block ties" (Huang 1993).

Determination of critical structural responses in terms of stresses and deflections in the slab track system is essential to mechanistic-based design as well as structural evaluation procedures. A review of the-state-of-the-art procedures in track analysis was first conducted and the fundamental assumptions and limitations were identified (AREMA 2001; Yen 2004). Finite-element models (FEM) have been successfully utilized to account for the effects of many practical conditions more realistically than theoretical solutions based on infinite slab and other idealized assumptions. With the introduction of three-dimensional [(3D) ABAQUS] (HKS 2000) FEM and all the promising features and results reported in the literature (Hammons 1998; Kim and Hjelmstad 2000; Kuo 1996), its applications on pavement/rail engineering become inevitable. Nevertheless, due to the required running-time and complexity of the FEM, 3D finite-element analysis cannot be easily implemented as a part of design or structural evaluation procedure.

In particular, the effects and sensitivity analysis of various design components of slab track systems were rarely investigated in the existing literature. In addition, the gaps between the available theoretical closed-form solutions and finite-element solutions are yet to be resolved. The importance of the study on the mesh fineness, convergence characteristics and element selections are often overlooked. Thus, the main objective of this study is to investigate their theoretical discrepancies, provide mesh fineness and element selection guidelines, as well as to develop a user-friendly interface program as a pre- and postprocessor of the ABAQUS program for future slab track analysis (Yen 2004).

Theoretical Solutions and Parameter Identification

Closed-Form Solutions

The fundamental theory due to Talbot, considering the track as a continuously and elastically supported beam subjected to a concentrated load, results in the following differential equation (Hay 1982):

$$E_s I_s \frac{d^4 y}{dx^4} = p \tag{1}$$

where $p = -uy$; p = upward pressure per unit length [FL^{-1}]; u = modulus of elasticity of the track support (track stiffness modulus) [FL^{-2}]; y = downward deflection [L]; and x = distance to any point on the deflection and bending moment curves [L]. The track stiffness modulus u is a lumped parameter combining tie, ballast, and subgrade stiffness in one term. E_s = modulus of elasticity of rail steel [FL^{-2}]; I_s = moment of inertia of the rail [L^4];

[1]Adjunct Assistant Professor, Dept. of Civil Engineering, Tamkang Univ., E729, #151 Ying-Chuan Rd., Tamsui, Taipei, Taiwan 251. E-mail: 123562@mail.tku.edu.tw

[2]Professor, Dept. of Civil Engineering, Tamkang Univ., E732, #151 Ying-Chuan Rd., Tamsui, Taipei, Taiwan 251 (corresponding author). E-mail: yinghaur@mail.tku.edu.tw

Note. Discussion open until October 1, 2007. Separate discussions must be submitted for individual papers. To extend the closing date by one month, a written request must be filed with the ASCE Managing Editor. The manuscript for this paper was submitted for review and possible publication on April 24, 2006; approved on October 17, 2006. This paper is part of the ***Journal of Transportation Engineering***, Vol. 133, No. 5, May 1, 2007. ©ASCE, ISSN 0733-947X/2007/5-288–297/$25.00.

(a)

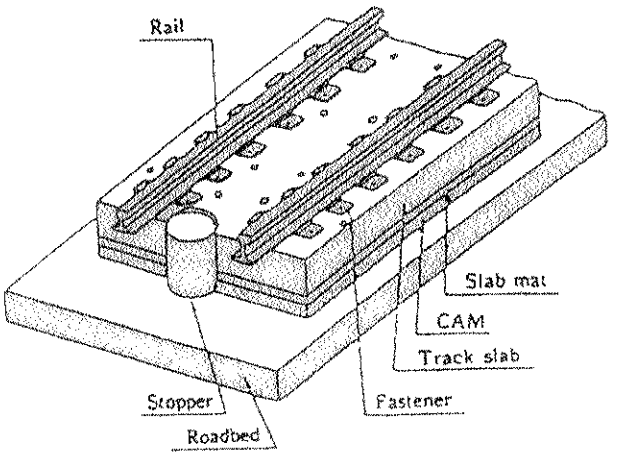

(b)

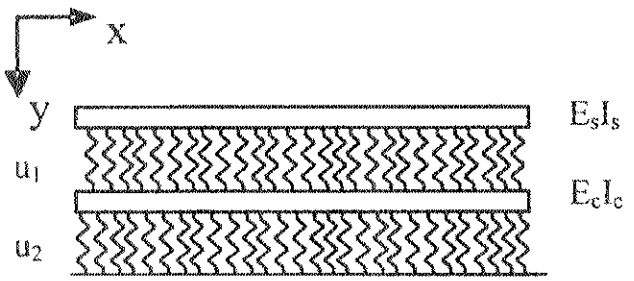

Fig. 1. Illustration and idealization of a slab track system: (a) a typical slab track system; (b) a double elastic beam system

and E_sI_s=flexural rigidity of the rail [F L^2]. Note that the primary dimensions are represented by [F] for force and [L] for length. This differential equation is satisfied by the following deflection equation and its successive derivatives:

$$y(x) = \frac{P}{8E_sI_s\lambda^3}\varphi_1(\lambda x)$$

$$M(x) = -E_sI_s\frac{d^2y}{dx^2} = \frac{P}{4\lambda}\varphi_3(\lambda x) \tag{2}$$

where p=concentrated wheel load [F]; M=bending moment [F L]; and $\lambda=\sqrt[4]{u/(4E_sI_s)}$=damping factor [L^{-1}]. Also note that φ_1 and φ_3 are Zimmerman functions: $\varphi_1(\lambda x)=e^{-\lambda x}(\cos\lambda x \sin\lambda x)$ and $\varphi_3(\lambda x)=e^{-\lambda x}(\cos\lambda x-\sin\lambda x)$.

Based on the idealization of two continuous beams on elastic foundations as shown in Fig. 1(b), the following differential equations are rederived (Hetenyi 1974; Wang 1987; Huang and Cheng 1993):

$$E_sI_s\frac{d^4y_1}{dx^4} = p_1$$

$$E_cI_c\frac{d^4y_2}{dx^4} + p_1 = p_2 \tag{3}$$

where $p_1=-u_1(y_1-y_2)$; $p_2=-u_2y_2$; p_1 and p_2 stand for the upward pressure per unit length on the rail and concrete slab [F L^{-1}]; y_1 and y_2 represent the deflections of the rail and concrete slab [L]; and u_1 and u_2 stand for the modulus of elasticity of the track support and that of the slab support [F L^{-2}], respectively. In addition, E_s is the modulus of elasticity of rail steel [F L^{-2}]; I_s=moment of inertia of the rail [L^4]; E_c=modulus of elasticity of concrete slab [F L^{-2}]; and I_c=moment of inertia of the concrete slab [L^4].

By assuming $l=u_1/(E_sI_s)$, $m=u_1/(E_cI_c)$, $n=u_2/(E_cI_c)$, and substituting $y_1=Ae^{\lambda x}$, $y_2=Be^{\lambda x}$ into the previous equation, one can obtain: $A\lambda^4+l(A-B)=0$ and $B\lambda^4-mA+(m+n)B=0$. By converting these two equations into $B/A=(\lambda^4+l)/l=m/(\lambda^4+m+n)$ and setting $U=\lambda^4$, the solutions of a second degree polynomial of U are obtained as U_1, $U_2=1/2(-(l+m+n)\pm\sqrt{(l+m+n)^2-4ln})$. Further, by assuming $\kappa=(-U_1/4)^{1/4}$ and $\omega=(-U_2/4)^{1/4}$, the following general solutions for the deflections of rail steel and concrete slab are obtained:

$$\begin{aligned} y_1 = {} & A_1e^{-\kappa x}\cos\kappa x + A_2e^{-\kappa x}\sin\kappa x + A_3e^{-\omega x}\cos\omega x + A_4e^{-\omega x}\sin\omega x \\ & + A_5e^{\kappa x}\cos\kappa x + A_6e^{\kappa x}\sin\kappa x + A_7e^{\omega x}\cos\omega x + A_8e^{\omega x}\sin\omega x \end{aligned}$$

$$\begin{aligned} y_2 = {} & B_1e^{-\kappa x}\cos\kappa x + B_2e^{-\kappa x}\sin\kappa x + B_3e^{-\omega x}\cos\omega x + B_4e^{-\omega x}\sin\omega x \\ & + B_5e^{\kappa x}\cos\kappa x + B_6e^{\kappa x}\sin\kappa x + B_7e^{\omega x}\cos\omega x + B_8e^{\omega x}\sin\omega x \end{aligned} \tag{4}$$

By applying the boundary conditions at the infinite distance, i.e., $x=\infty$, $y_1(x)=0$ and $y_2(x)=0$, one can obtain $A_5=A_6=A_7=A_8=0$ and $B_5=B_6=B_7=B_8=0$. Further, by applying the following boundary conditions for a concentrated load located at the origin: $dy_1/dx=0$, $dy_2/dx=0$, $2E_sI_s(d^3y_1/dx^3)=P$, and $d^3y_2/dx^3=0$, after assuming $\xi=(U_1+l)/l$ and $\eta=(U_2+l)/l$ one can obtain the coefficients as $A_1=A_2=\epsilon\rho^*/\kappa^3$, $A_3=A_4=-\rho^*/\omega^3$, $B_1=B_2=\rho^*/\kappa^3$, and $B_3=B_4=-\rho^*/\omega^3$, where $\epsilon=\eta/\xi=(U_2+l)/(U_1+l)$ and $\rho^*=P/(4(\epsilon-1)\cdot 2E_sI_s)$. Thus, the following deflection equations and its successive derivatives satisfy the aforementioned differential equations:

$$y_1 = \left[\frac{\varepsilon}{\kappa^3}\varphi_1(\kappa x) - \frac{1}{\omega^3}\varphi_1(\omega x)\right]\rho^*$$

$$y_2 = \eta\left[\frac{1}{\kappa^3}\varphi_1(\kappa x) - \frac{1}{\omega^3}\varphi_1(\omega x)\right]\rho^* \tag{5}$$

$$M_1 = -2E_sI_s\left[-\frac{\varepsilon}{\kappa}\varphi_3(\kappa x) + \frac{1}{\omega}\varphi_3(\omega x)\right]\rho^*$$

$$M_2 = -2E_cI_c\eta\left[-\frac{1}{\kappa}\varphi_3(\kappa x) + \frac{1}{\omega}\varphi_3(\omega x)\right]\rho^* \tag{6}$$

where, y_1 and y_2=deflections of the rail and concrete slab; M_1 and M_2=bending moments of the rail and concrete slab [F L], respectively; and $\varphi_1(\kappa x)$, $\varphi_3(\kappa x)$, $\varphi_1(\omega x)$, and $\varphi_3(\omega x)$=Zimmerman functions as previously defined. The maximum deflections (δ_s and δ_c) and bending moments (M_s and M_c) occurring at the point of load application where $x=0$ are listed as follows:

$$\delta_s = \left[\frac{\varepsilon}{\kappa^3} - \frac{1}{\omega^3}\right]\frac{1}{4(\varepsilon-1)}\frac{P}{2E_sI_s}$$

$$\delta_c = \eta\left[\frac{1}{\kappa^3} - \frac{1}{\omega^3}\right]\frac{1}{4(\varepsilon-1)}\frac{P}{2E_sI_s} \tag{7}$$

$$M_s = \left[\frac{\varepsilon}{\kappa} - \frac{1}{\omega}\right]\frac{1}{4(\varepsilon - 1)}P$$

$$M_c = \eta\left[\frac{1}{\kappa} - \frac{1}{\omega}\right]\frac{1}{4(\varepsilon - 1)}\frac{E_c I_c}{E_s I_s}P \tag{8}$$

The critical stress of the rail or concrete slab can then be determined by $\sigma = Mc/I$, where σ = critical stress of the rail or concrete slab [F L^{-2}]; M = maximum bending moment of the rail or the concrete slab [F L]; c = distance from the base of the rail or concrete slab to its neutral axis [L]; and I = moment of inertia of the rail or concrete slab [L^4].

Identification of Dominating Mechanistic Variables

Based on the elastic beam theory and the theory of two continuous beams on elastic foundations, the following parameters are subsequently defined:

$$l_r = \sqrt[4]{\frac{E_s I_s}{u_1}} \tag{9}$$

$$l_{rk} = \sqrt[4]{\frac{E_c I_c}{u_1}} \tag{10}$$

$$l_k = \sqrt[4]{\frac{E_c I_c}{u_2}} \tag{11}$$

where l_r is defined as the radius of relative stiffness of the rail and track support [L]; l_{rk} is defined as the radius of relative stiffness of the concrete slab and track support [L]; and l_k is defined as the radius of relative stiffness of the concrete slab and slab support [L].

Applying the principles of dimensional analysis to the solutions of elastic beam theory and the maximum deflection and bending moment relationships of the theory of two continuous beams on elastic foundations, i.e., Eqs. (2), (7), and (8), the following concise relationships are obtained:

$$\frac{yE_s I_s}{Pl_r^3}, \frac{M}{Pl_r} = f_1\left(\frac{x}{l_r}\right) \tag{12}$$

$$\frac{\delta E_s I_s}{Pl_r^3}, \frac{M}{Pl_r} = f_2\left(\frac{l_{rk}}{l_r}, \frac{l_k}{l_r}\right) \tag{13}$$

where y = downward deflection [L]; x = distance to any point on the deflection and bending moment curves [L]; δ = maximum deflection of the rail or concrete slab [L]; M = maximum bending moment of the rail or concrete slab [F L]. Also note that all the variables in both sides of equations are dimensionless. $(\delta E_s I_s)/(Pl_r^3)$ and $M/(Pl_r)$ are the normalized deflection and normalized moment parameters, respectively.

Finite-Element Model Idealizations

According to earlier literature (Kuo 1996; Bao 1998), the well-known 3D finite-element program (ABAQUS) (HKS 2000) was selected for this study. Various elements will be carefully chosen to simulate different components of the slab track system. In particular, 3D shell and 3D solid (block) elements, beam elements, and spring elements will be used to model concrete slabs, rails, and various rail fastenings as well as the subgrade support, respectively. Recommendations for element selections are subsequently provided.

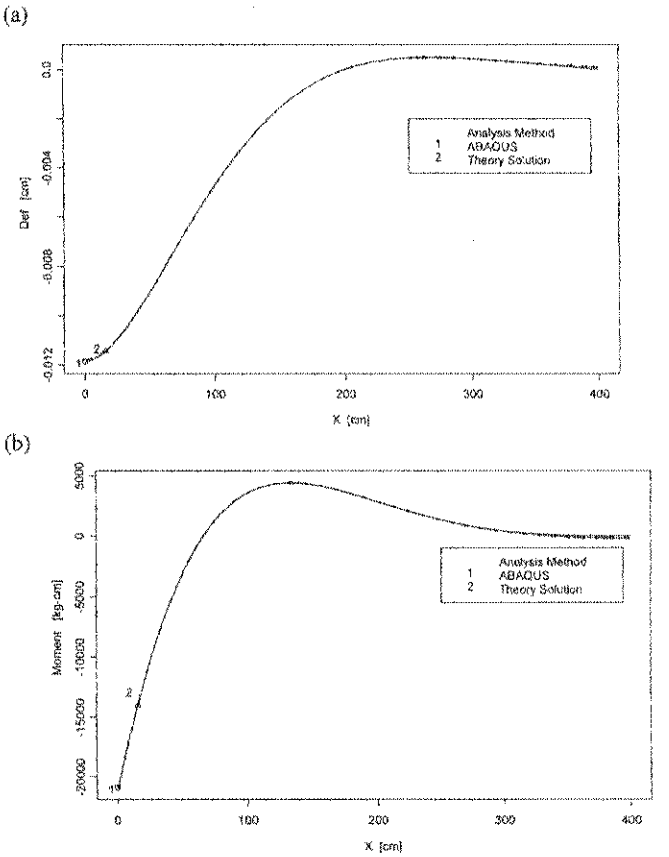

Fig. 2. Comparison of ABAQUS solutions with closed-form solutions: (a) rail deflection; (b) rail bending moment

Two-Dimensional Model Building and Verifications

Various beam elements such as B21, B31, B31H, B32, B32H, and B31OS defined in the ABAQUS library can be used to model the rails. According to the literature, using the two-node linear beam element types B21 and B31 can adequately achieve the desired accuracy while considering the efficiency of the required computation time and resources. Assuming a longitudinal rail resting on a Winkler foundation with the following pertinent input parameters: P=9.81 kN, E_s=206 GPa, I_s=3,090 cm^4, u=49.05 MPa, the infinite rail length L=400 cm, the spacing of rail support (or fastenings) s=0.58 m, the beam element type B21 was used to model the rails and the foundation was modeled as SPRING elements. Using a very fine mesh with 400 beam elements and a symmetry option, the resulting ABAQUS rail deflection and bending moments were compared to the closed-from solutions with excellent agreements as shown in Fig. 2.

In addition, assuming two continuous beams on elastic foundations with the following parameters: P=49.05 kN, E_s=226 GPa, I_s=4,000 cm^4, u_1=241 MPa, E_c=245 GPa, I_c=1.86E+05 cm^4, u_2=130 MPa, the infinite rail length L=400 cm, the spacing of the rail support (or rail fastenings) s=0.60 m, the beam element type B21 and SPRING elements were used to model the rails and the foundation, respectively. Using a very fine mesh with 400 beam elements and a symmetry

option, the resulting ABAQUS maximum deflections and bending moments are $y_1=0.03178$ cm, $y_2=0.01558$ cm, $M_1=8{,}221$ N m, and $M_2=5{,}990$ N m, as compared to the corresponding closed-form solutions $y_1=0.03091$ cm, $y_2=0.01531$ cm, $M_1=8{,}562$ N m, and $M_2=5{,}987$ N m.

3D Model Building and Element Selections

As for 3D FEM analyses, the beam element type B31 was used to model the rails in this study. Different from the earlier literature (Kuo 1996; Bao 1998), the connector element type JOINTC was adopted to model the effects of elastic constraints and load transfers of the rail fastening systems (Yen 2004). This element can provide the connection between two nodes while allowing the inputs of a spring constant and the dashpot damping. In addition, to avoid potential stress concentration this element is also connected to a shell element with rigid elements RB3D2 on each node was also used to uniformly distribute the load to the concrete slab. The subgrade was modeled as a Winkler foundation or dense liquid foundation in the normal fashion. As identical results are obtained using either SPRING elements or the Foundation option, the latter was chosen to model the subgrade due to its ease of use.

Various 3D shell and 3D solid (block) elements are used to model concrete slabs. A brief summary of the characteristics of the 3D shell and 3D solid elements from the ABAQUS library considered in this study is available (Hammons 1998; Wu 2003). These include both linear and quadratic elements employing both full and reduced integration. The number of nodes, the degree of freedom, and the number of Gauss integration points per element indicating their relative complexity and required computation time are also summarized. Two types of thin shell elements (4 node, 8 node, and 9 node) are considered: those satisfy the thin shell theory (the Kirchhoff constraint) analytically and those converge to thin shell theory numerically as the thickness decreases. The selected 3D solid (brick) elements (8 node, 20 node, and 21–27 node) include first-order (linear) and second-order (quadratic) interpolation elements. Second-order elements provide higher accuracy than first-order elements and are very effective in bending-dominated problems.

The element types S4 and S4R are general-purpose shells. The S4R5, S8R5, and S9R5 shell elements, which impose the Kirchhoff constraint numerically, are intended for the analysis of thin shells, whereas the element type S8R should be used only for thick shells. Element type C3D20 has 27 integration points, while C3D20R has only eight integration points. The C3D27 and C3D27R elements are variable node elements, of which the number of nodes can be reduced to 21 (or any number between 21 and 27) per element by removing the interior node from each of the faces of the element as desired. Reduced integration reduces the computation time through the use of a lower-order integration to form the element stiffness. Generally speaking, the accuracy achieved with full versus reduced integration first-order elements is largely dependent on the nature of the problem. For second-order elements, reduced-integration elements generally yield more accurate results than the corresponding fully integrated elements (HKS 2000; Hammons 1998).

Mesh Fineness and Convergence Study

A systematic approach was utilized and implemented in a VISUAL BASIC software package to study the effects of mesh fineness and element selections using the ABAQUS finite-element program. This program was developed to automatically construct FEM models, generate the input files, conduct the runs, as well as summarize the results. The convergence characteristics of various 3D shell and 3D solid elements are investigated. Several guidelines in mesh fineness and element selections are recommended.

Definition of Mesh Fineness and Mesh Generation

Mesh generation in the horizontal direction generally includes the following steps: The consideration of applicable symmetry option, generation of finer mesh at the loaded area (Zone I) and at its neighborhood area (Zone II), and progressively increasing to coarser mesh further away (Zone III) for efficiency consideration. The horizontal mesh fineness is defined as the ratio of the length of the loaded area to the selected element length throughout this study. In addition, Zones I and II were chosen to have the same mesh fineness.

The length of the Zone II in the longitudinal direction was set to three times the spacing of the rail fastenings, whereas the length of the Zone II in the transverse direction was chosen as two times the length of the loaded area in this study for consistency and efficiency considerations (Yen 2004). The mesh of Zone III was decided as four times coarser than Zone I (Wu 2003; Lee et al. 2004). Vertical mesh fineness was defined as the number of evenly divided layers for practical model building concern in this study.

Deflection Convergence Characteristics

A single finite slab track system resting on a Winkler foundation under a concentrated load with the following input parameters: $P=9.81$ kN, $E_s=235$ GPa, $I_s=2{,}000$ cm^4, $u_1=105$ MPa, finite slab/rail length=4.8 m, finite slab width $W=3.84$ m, slab thickness $h_c=16$ cm, $E_c=19.6$ GPa, $u_2=56.8$ MPa, the size of rail fastenings 24×24 cm^2, the spacing of the rail support (or rail fastenings) $s=0.60$ m was chosen for the mesh fineness study.

For higher accuracy consideration, same horizontal mesh fineness of up to 12 for Zones I and II was considered. The slab thickness was subdivided into up to four sublayers for vertical mesh fineness study. The deflection convergence characteristics of various FEM element types were investigated. Fig. 3 depicts the rail and slab deflection convergence characteristics using B31 beam elements with 3D shell elements. In which, deflection ratio was defined as the ratio of the resulting FEM deflections to the corresponding closed-form solutions. Horizontal mesh fineness ranges from 1 to 12. The element types S4, S4R, S4R5, S8R, S8R5, and S9R5 all resulted in very close deflection values. Generally speaking, the FEM rail deflections are about 16% lower than the closed-form solutions, whereas the FEM slab deflections are about 10% higher than the closed-form solutions.

Figs. 4 and 5 display the rail and slab deflection convergence characteristics using B31 beam elements with 3D solid elements. Deflection ratio and horizontal mesh fineness are defined the same as before. The vertical mesh fineness within each plot is defined to evenly divide the slab thickness into one to four sublayers. Using vertical mesh fineness of one (or one layer) was proved inadequate and should be avoided for 3D solid elements. Especially for the C3D8 and C3D8R elements, the resulting deflection ratios can be very different from those obtained for the other 3D solid elements regardless of increasing horizontal mesh fineness

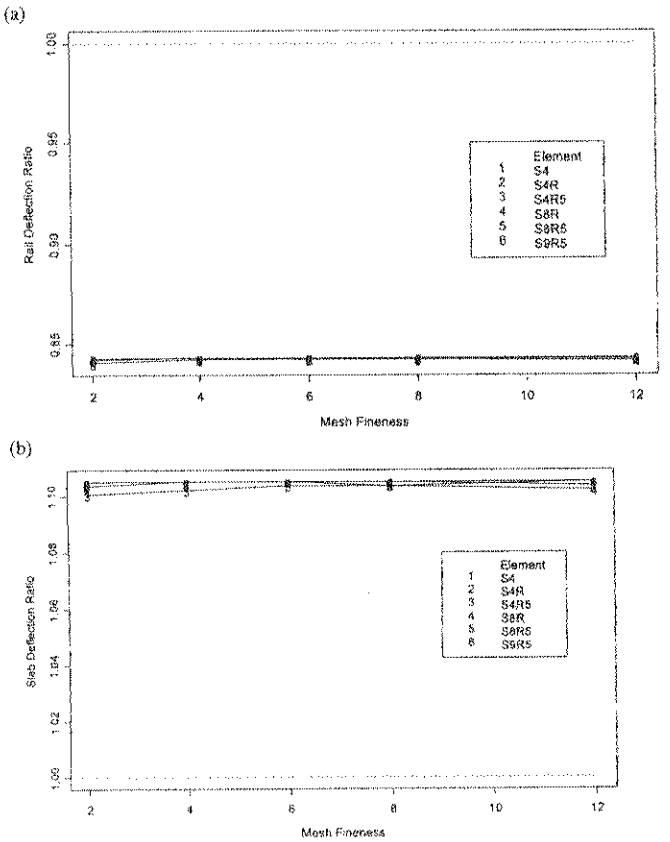

Fig. 3. Rail and slab deflection convergence characteristics: (a) rail deflection; (b) slab deflection (B31 beam elements with 3D shell elements)

when vertical mesh fineness is set to one. By increasing both mesh fineness, the resulting deflections of 8-node elements are very close to 20- and 27-node elements.

Generally speaking, the rail deflections of all 3D solid elements are about 16% lower than the closed-form solutions, whereas the slab deflections are approximately 10% higher than the closed-form solutions. These results may be explained by their theoretical discrepancies in allowing or disallowing compressions within elements. To achieve high accuracy and computation efficiency, it was recommended that element type C3D20 with a horizontal mesh fineness of 3 and a vertical mesh fineness of 3 be selected for further analysis.

Verification of Dominating Mechanistic Variables

As shown in Table 1, various FEM runs were conducted and compared to the closed-form solutions given in Eq. (13) to numerically verify the relationship for a continuously and elastically supported beam subjected to a concentrated load. Keeping the dimensionless parameter x/l_r constant while changing other input variables, the normalized deflection $(yE_sI_s)/(Pl_r^3)$ and the normalized moment $M/(Pl_r)$ remain unchanged. If the rail is limited in length, the normalized maximum responses will depend on the dimensionless parameter L/l_r alone based on the principles of dimensional analysis, where L=finite rail length, [L].

Similarly, a series of FEM runs were conducted to numerically verify the relationship for a continuously and elastically supported beam subjected to a uniformly distributed load (q). Keeping the dimensionless parameter a/l_r constant while changing other input variables, the normalized maximum responses remain unchanged as shown in Table 2. Table 3 displays some cases analyzed to numerically verify the relationship given in Eq. (13) for two continuous beams on elastic foundations. By keeping these two dimensionless parameters (l_{rk}/l_r and l_k/l_r) constant, the normalized maximum responses remain unchanged as well. Subsequently, the following concise relationship is identified to account the theoretical differences for a finite rail resting on elastic foundations subjected to a uniformly distributed load (Yen 2004):

$$\frac{\delta E_s I_s}{P l_r^3}, \frac{M}{P l_r} = f_3\left(\frac{a}{l_r}, \frac{l_{rk}}{l_r}, \frac{l_k}{l_r}, \frac{L}{l_r}\right) \tag{14}$$

Implementation and Verification of an Alternative Stress Analysis Procedure

A slab track system consists of the rails, rail-pad-fastener systems, concrete slab, and subgrade. Traffic loadings are applied to the rails connected directly to the concrete slab or through rubber booted block ties. A different gear load configuration, a finite slab width or length, and a second bonded or unbonded layer may also result in different degrees of stress reduction. The effect of a temperature differential or moisture gradient (linear or nonlinear) may alter the magnitude of critical stresses. Thorough treatments of various combinations of all such conditions are very challenging due to the complexity and vast amount of required computation time in 3D FEM analysis.

To allow the analysis of more practical loading conditions, the substructures of a slab track system as shown in Fig. 6(a) were separately analyzed (Yen 2004). By applying the concept of a free body diagram as shown in Fig. 6(b), several additional dimensionless parameters were identified based on the aforementioned elastic beam theories and the plate theory to account for the effects of multiple steel wheel loads, the spacing of rail-fastenings, and the concrete slab. Several series of 3D FEM factorial runs were conducted based on the relationship given by Eq. (14). Separate databases were created using beam element type B31 and C3D20 solid elements with a horizontal mesh fineness of 3 and a vertical mesh fineness of 3. Various prediction models for stress adjustments were developed using projection pursuit regression techniques proposed by Lee and Darter (1994). Together with the existing two-dimensional and 3D FEM prediction models for concrete pavements (Lee et al. 1996; 2004), the following systematic stress analysis procedure was proposed (Yen 2004):

1. Input the axle load (P) and the pertinent parameters of a slab track system;
2. Convert the input parameters into dominating mechanistic variables (l_{rk}/l_r, l_k/l_r, s/l_r, and x/l_r);
3. Determine the maximum reaction force of fasteners (F_0), $F_0=PR_{F_0}$, where $R_{F_0}=f_1(l_{rk}/l_r, l_k/l_r, s/l_r)$;
4. Calculate each reaction force of fasteners (F_i), $F_i=F_0R_{F_i}R_{D_a}$, in which $R_{F_i}=f_2(x/l_r)$, $R_{D_a}=f_3(D_a/l_r)$, and D_a=tandem axle spacing;
5. Convert each F_i into uniform load (q_i) applied on the concrete slab and calculate the corresponding interior slab stress (σ_{wi}) using Westergaard's closed-form solution;
6. Determine the critical slab stress, $\sigma_i=\Sigma_{i=0}^{n}(\sigma_{wi}R_{D_0})$, where $R_{D_0}=f_3(a/l, D_0/l)$ is the stress reduction at a distance (D_0) away from the critical location; and
7. Make critical stress adjustment due to the effects of finite

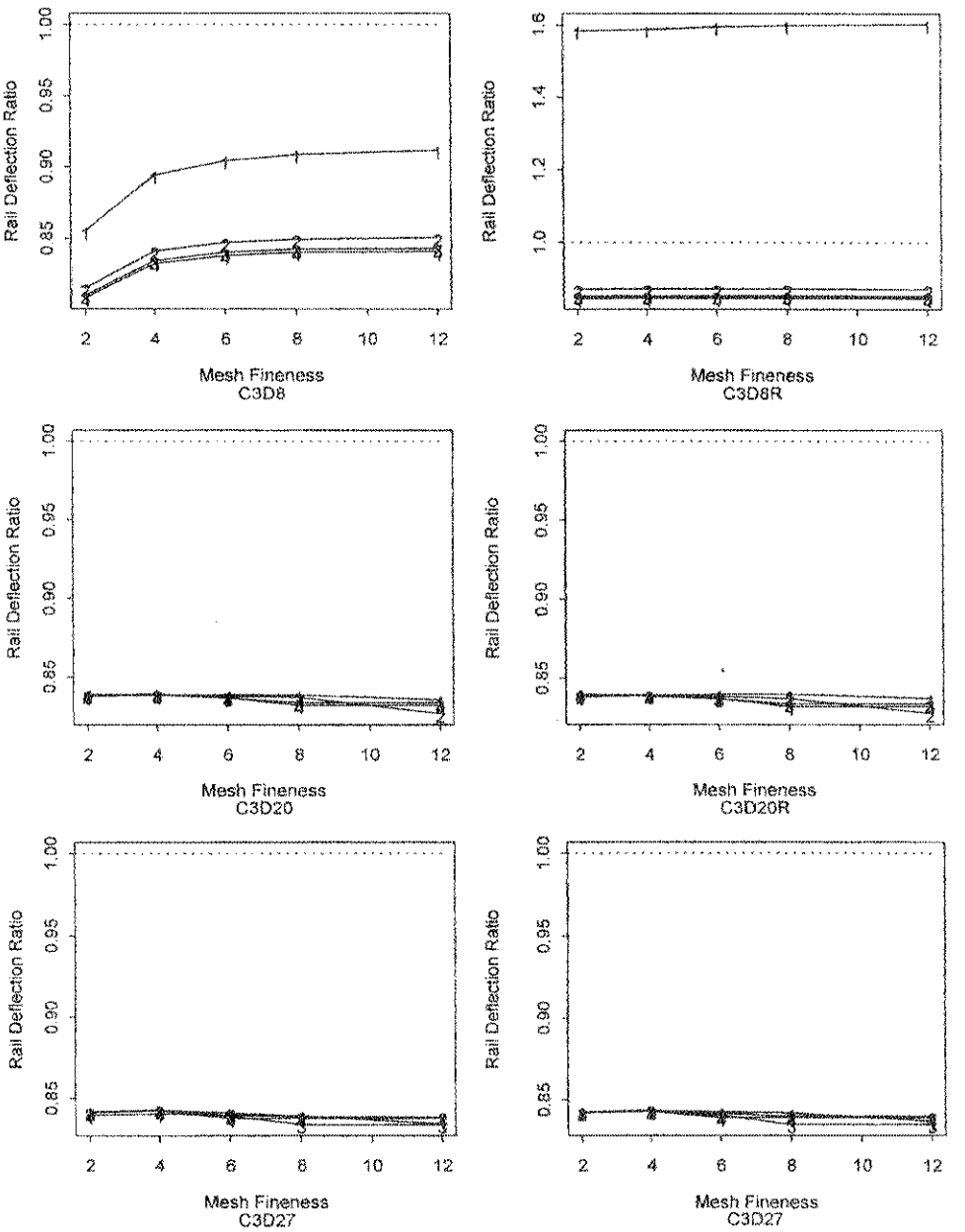

Fig. 4. Rail deflection convergence characteristics (3D solid elements)

slab length (L_c) and slab width (W_c) and the rail spacing (t), $\sigma_{FEM}=\sigma_i R_{LW} R_t$, where $R_{LW}=f_4(a/l, L_c/l, W_c/l)$ and $R_t=f_5(a/l, t/l)$.

Note that the adjustment factors (f_1–f_5) stand for the predictive functions determined by the dominating mechanistic variables listed inside the parentheses.

Finally, the proposed procedure has been implemented in an EXCEL spreadsheet file named TKUTRACK using the VISUAL BASIC FOR APPLICATIONS software to facilitate future routine slab track analyses. An example input and output screen of the TRKTRACK program is given in Fig. 7 for illustration purposes. The applicability of this Windows-based prototype program was further verified through a completely different database generated using different input parameters (Yen 2004). A partial list of the prediction and verification of critical slab stresses is given in Table 4. As shown in Fig. 8, very good agreement has been observed when comparing the TKUTRACK predicted stresses versus the resulting ABAQUS slab stresses.

More detailed information regarding the tentative applications of the proposed analytical procedure can be found in the literature (Yen 2004).

Conclusions

The idealized theoretical solutions for a continuously and elastically supported beam and two continuous beams on elastic foundations subjected to a concentrated load were first investigated. Together with the principles of dimensional analysis as well as its similarity to a rigid pavement system, several dominating mechanistic variables were identified and numerically verified. A sys-

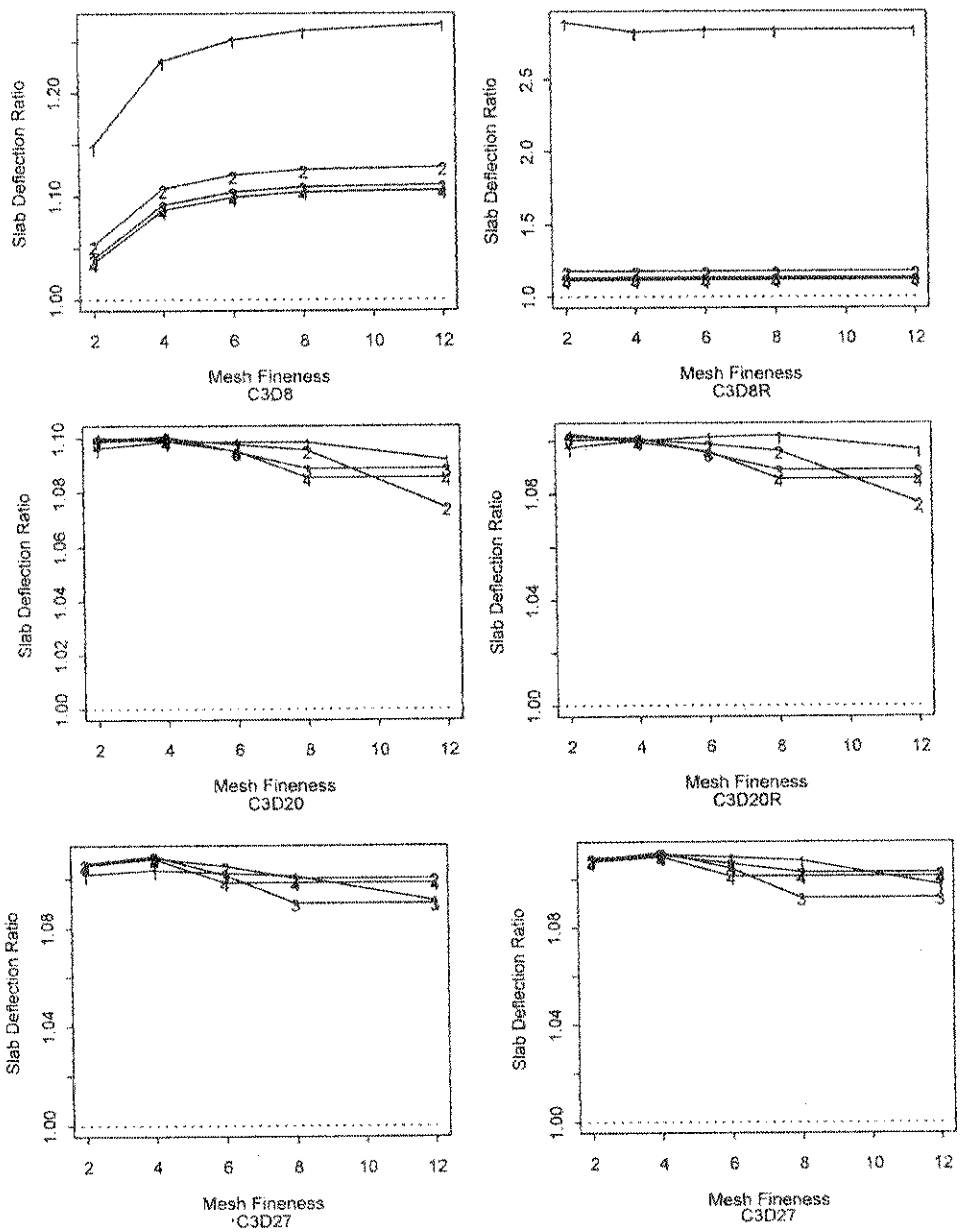

Fig. 5. Slab deflection convergence characteristics (3D solid elements)

Table 1. Verification of the Normalized Solutions for a Continuously and Elastically Supported Beam Subjected to a Concentrated Load

							Theory		ABAQUS	
$\frac{x}{l_r}$	x (cm)	E_s (GPa)	I_s (cm^4)	u (MPa)	l_r (cm)	λ (cm^{-1})	$\frac{yE_sI_s}{Pl_r^3}$	$\frac{M}{Pl_r}$	$\frac{yE_sI_s}{Pl_r^3}$	$\frac{M}{Pl_r}$
0	0	196.2	2,050	98.10	45	0.0157	0.354	0.354	0.358	0.347
0	0	215.8	4,712	78.48	60	0.0118	0.354	0.354	0.358	0.348
0	0	237.4	6,537	49.05	75	0.0094	0.354	0.354	0.357	0.349
0.4	24	215.8	4,712	78.48	60	0.0118	0.330	0.182	0.332	0.180
0.4	30	237.4	6,537	49.05	75	0.0094	0.330	0.181	0.332	0.180
0.4	44	287.2	5,000	9.81	110	0.0064	0.330	0.182	0.344	0.184
0.8	36	196.2	2,050	98.10	45	0.0157	0.277	0.062	0.277	0.061
0.8	60	237.4	6,537	49.05	75	0.0094	0.277	0.062	0.278	0.061
0.8	72	261.1	4,929	19.62	90	0.0079	0.277	0.062	0.281	0.062

Table 2. Verification of the Normalized Solutions for a Continuously and Elastically Supported Beam Subjected to a Uniform Distributed Load

							Theory		ABAQUS	
$\frac{a}{l_r}$	P (kN)	a (cm)	E_s (GPa)	I_s (cm^4)	u (MPa)	l_r (cm)	$\frac{\delta E_s I_s}{P l_r^3}$	$\frac{M}{P l_r}$	$\frac{\delta E_s I_s}{P l_r^3}$	$\frac{M}{P l_r}$
0.1	9.81	4	196.2	1,280	98.1	40	0.353	0.341	0.357	0.338
0.1	14.715	6	215.8	4,713	78.48	60	0.353	0.341	0.357	0.339
0.1	19.62	8	237.4	8,463	49.05	80	0.353	0.341	0.357	0.340
0.3	29.43	12	196.2	1,280	98.1	40	0.352	0.317	0.356	0.316
0.3	44.145	18	215.8	4,713	78.48	60	0.352	0.317	0.356	0.316
0.3	58.86	24	237.4	8,463	49.05	80	0.352	0.317	0.355	0.316
0.5	49.05	20	196.2	1,280	98.1	40	0.350	0.295	0.353	0.293
0.5	73.575	30	215.8	4,713	78.48	60	0.350	0.295	0.353	0.293
0.5	98.1	40	237.4	8,463	49.05	80	0.350	0.295	0.353	0.294

Table 3. Verification of the Dominating Mechanistic Variables for Two Continuous Beams on Elastic Foundations

									Theory		ABAQUS			
$\frac{l_r}{l_{r,0}}$	$\frac{I_c}{I_h}$	P (kN)	E_s (GPa)	I_s (cm^4)	u_1 (MPa)	E_c (GPa)	I_c (cm^4)	u_2 (MPa)	$\frac{\delta_1 E_s I_s}{P l_r^3}$	$\frac{\delta_2 E_s I_s}{P l_r^3}$	$\frac{\delta_1 E_s I_s}{P l_r^3}$	$\frac{\delta_2 E_s I_s}{P l_r^3}$	$\frac{M_1}{P l_r}$	$M_2/P l_r$
0.690	0.615	147.2	206	8,000	644	34.3	212,000	408	0.634	0.298	0.652	0.300	0.384	0.242
0.690	0.615	98.1	216	6,000	416	29.4	195,000	264	0.634	0.298	0.650	0.300	0.385	0.242
0.690	0.615	49.05	226	4,000	241	24.5	163,000	153	0.634	0.298	0.649	0.300	0.385	0.242
0.690	0.533	196.2	196	10,000	941	41.2	211,000	337	0.803	0.469	0.824	0.474	0.398	0.311
0.690	0.533	147.2	206	8,000	644	34.3	212,000	230	0.803	0.469	0.822	0.474	0.399	0.311
0.690	0.533	98.1	216	6,000	416	29.4	195,000	149	0.803	0.469	0.822	0.475	0.399	0.311
0.667	0.571	98.1	216	6,000	416	29.4	223,000	225	0.668	0.331	0.684	0.334	0.386	0.279
0.667	0.571	49.05	226	4,000	241	24.5	186,000	130	0.668	0.331	0.683	0.334	0.387	0.278
0.667	0.571	9.81	235	2,000	105	19.6	122,000	57	0.668	0.331	0.683	0.334	0.387	0.278
0.667	0.533	98.1	216	6,000	416	29.4	223,000	170	0.747	0.412	0.765	0.416	0.393	0.314
0.667	0.533	49.05	226	4,000	241	24.5	186,000	99	0.747	0.412	0.765	0.417	0.393	0.314
0.667	0.533	9.81	235	2,000	105	19.6	122,000	43	0.747	0.412	0.766	0.419	0.394	0.313

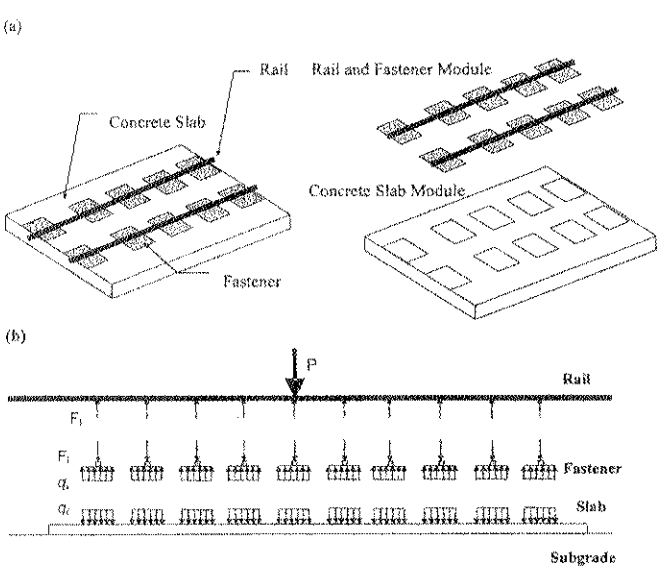

Fig. 6. Illustration of the (a) substructures; (b) the free body diagrams of a slab track system

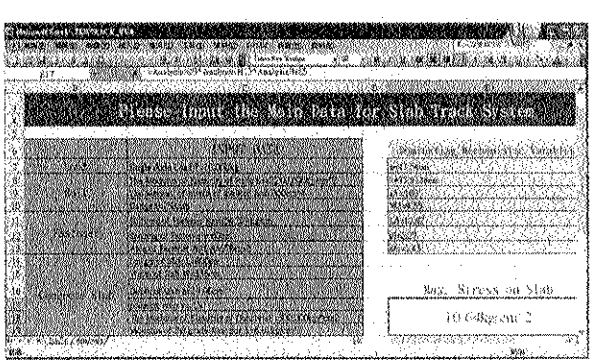

Fig. 7. Example input and output screen of the TKUTRACK program

Table 4. Prediction and Verification of Critical Slab Stresses (Partial List)

P (kN)	E_s (GPa)	I_s (cm^4)	u_1 (MPa)	E_c (GPa)	I_c (cm^4)	u_2 (MPa)	h_c (cm)	k (MN/m^3)	W (m)	t (m)	Slab stress ABAQUS (MPa)	Slab stress Predicted (MPa)
9.81	235	2,000	105	20	312,340	57	22	26.4	3.52	1.76	0.11	0.11
14.715	235	2,000	105	20	171,070	57	18	26.4	3.52	1.76	0.21	0.21
14.715	235	2,000	105	20	50,688	57	12	26.4	3.52	1.76	0.36	0.37
29.43	235	2,000	105	20	312,340	57	22	26.4	3.52	1.76	0.33	0.33
29.43	235	2,000	105	20	120,150	57	16	26.4	3.52	1.76	0.49	0.50
29.43	235	2,000	105	20	50,688	57	12	26.4	3.52	1.76	0.72	0.74
49.05	226	4,000	241	25	55,296	130	12	55.5	3.84	1.92	1.11	1.14
49.05	226	4,000	241	25	702,460	130	28	55.5	3.84	1.92	0.34	0.35
73.575	226	4,000	241	25	864,000	130	30	55.5	3.84	1.92	0.47	0.47
73.575	226	4,000	241	25	702,460	130	28	55.5	3.84	1.92	0.51	0.52
98.1	216	6,000	416	29	756,000	225	30	109.6	3.36	1.92	0.60	0.60
147.15	226	4,000	241	25	864,000	130	30	55.5	3.84	1.92	0.95	0.94
147.15	206	8,000	644	34	497,580	347	28	209.5	2.72	1.36	0.96	0.98
196.2	196	10,000	941	41	304,650	508	26	400.5	2.08	1.36	1.46	1.49
196.2	196	10,000	941	41	380,500	508	28	400.5	2.08	1.36	1.36	1.33
220.725	206	8,000	644	34	612,000	347	30	209.5	2.72	1.36	1.34	1.33
220.725	206	8,000	644	34	497,580	347	28	209.5	2.72	1.36	1.45	1.47
294.3	216	6,000	416	29	756,000	225	30	109.6	3.36	1.36	1.79	1.79
441.45	206	8,000	644	34	612,000	347	30	209.5	2.72	1.36	2.68	2.65
588.6	196	10,000	941	41	380,500	508	28	400.5	2.08	1.04	4.07	4.00

tematic approach was utilized and implemented in a VISUAL BASIC software package to study the effects of mesh fineness and element selections using the ABAQUS finite-element program. This program was developed to automatically construct FEM models, generate the input files, conduct the runs, as well as summarize the results. The convergence characteristics of various 3D shell and 3D solid elements were investigated.

Generally speaking, the FEM rail deflections are about 16% lower than the closed-form solutions, whereas the FEM slab deflections are about 10% higher than the closed-form solutions for the cases analyzed. To achieve high accuracy and computation efficiency, it was recommended that element type C3D20 with a horizontal mesh fineness of 3 and a vertical mesh fineness of 3 be selected. This study strives to bridge the gap between the closed-form theoretical solutions and the numerical results obtained from 3-D FEM analyses so as to expand its applicability to various practical track conditions more realistically.

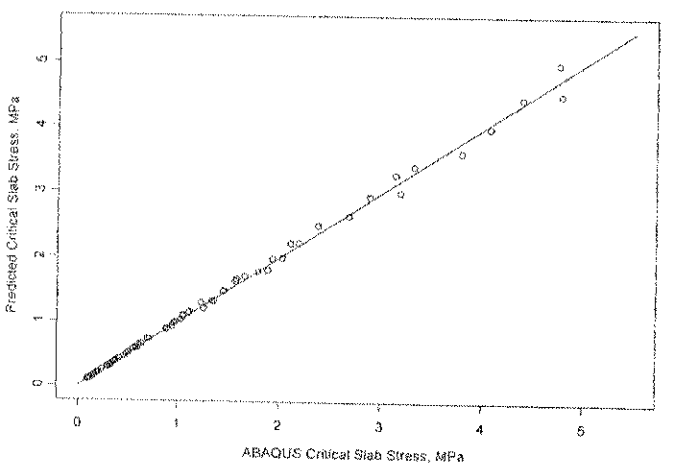

Fig. 8. Verification of the critical slab stress for TKUTRACK and ABAQUS

Acknowledgments

This study was sponsored by National Science Council of Taiwan, under the project titled "Development and Application of Automatic Stress Program for Slab Track," Phase I (NSC 91-2211-E-032-021) and Phase II (NSC92-2211-E032-013).

References

American Railway Engineering and Maintenance-of-Way Association (AREMA). (2001). *AREMA manual for railway engineering*, Landover, Md.

Bao, Y. L. (1998). "Three-dimensional stability/lateral shift analysis of continuous welded rail (CWR) track and innovative methods to enhance CWR track performance." Ph.D. dissertation, Univ. of Illinois, Urbana, Ill.

Bilow, D. N., and Randich, G. M. (2000). "Slab track for the next 100 years." *Proc., American Public Transportation Association 2000 Rail Transit Conf.*

Hammons, M. I. (1998). "Advanced pavement design: Finite element modeling for rigid pavement joints." *Rep. No. II: Model Development, DOT/FAA/AR-97-7*, Federal Aviation Administration, U.S. Dept. of Transportation.

Hay, W. W. (1982). *Railroad engineering*, Wiley, New York.

Hetenyi, M. (1974). *Beams on elastic foundation: Theory with applications in the fields of civil and mechanical engineering*, University of Michigan Press, Ann Arbor, Mich.

Hibbitt, Karlsson, and Sorensen, Inc. (HKS). (2000). *ABAQUS/standard user's manual*, Vols. I and II, version 6.2.1, Pawtucket, R.I.

Huang, M. J., and Cheng, S. F. (1993). *Modern railway engineering*, Wensheng Bookstore, Taipei, Taiwan (in Chinese).

Huang, Y. H. (1993). *Pavement analysis and design*, Prentice-Hall, Englewood Cliffs, N.J.

Kim, J., and Hjelmstad, K. (2000). "Three-dimensional finite element analysis of multi-layered systems: Comprehensive nonlinear analysis of rigid airport pavement systems." *Federal Aviation Administration DOT 95-C-001, COE Rep. No. 10*, Univ. of Illinois at Urbana-Champaign, Urbana, Ill.

Kuo, C. M. (1996). "Characteristics and design requirements of a slab track system." *Final Rep. No. NSC85-2221-E-006-058*, National Cheng Kung Univ., Tainan, Taiwan (in Chinese).

Lee, Y. H., Bair, J. H., Lee, C. T., Yen, S. T., and Lee, Y. M. (1996). "Modified Portland cement association stress analysis and thickness design procedures." *Transportation Research Record. 1568*, Transportation Research Board, Washington, D.C.

Lee, Y. H., and Darter, M. I. (1994). "New predictive modeling techniques for pavements." *Transportation Research Record. 1449*, Transportation Research Board, Washington, D.C., 234–245.

Lee, Y. H., Wu, H. T., and Yen, S. T. (2004). "Parameter studies and verifications on three-dimensional finite element analysis of rigid pavements." *Can. J. Civ. Eng.*, 31(5), 782–796.

Wang, C. C. (1987). *Analysis of railway dynamics*, Southwest Jiaotong Univ. Chengdu, P.R. China (in Chinese).

Wu, H. T. (2003). "Parameter analysis and verification for jointed concrete pavements." Master's thesis, Tamkang Univ., Taiwan (in Chinese).

Yen, S. T. (2004). "Development and application of automatic stress analysis program for slab track." Ph.D. dissertation, Tamkang Univ., Taiwan (in Chinese).